Geometrically exact initially curved Kirchhoff's planar elasto-plastic beam

Ismar Imamovic[*1], Adnan Ibrahimbegovic[2a] and Emina Hajdo[1b]

[1]Faculty of Civil Engineering, University of Sarajevo, Sarajevo, Bosnia and Herzegovina
[2]University of Technology of Compiegne/Sorbonne University Alliance, Compiegne, France

Abstract. In this paper we present geometrically exact Kirchhoff's initially curved planar beam model. The theoretical formulation of the proposed model is based upon Reissner's geometrically exact beam formulation presented in classical works as a starting point, but with imposed Kirchhoff's constraint in the rotated strain measure. Such constraint imposes that shear deformation becomes negligible, and as a result, curvature depends on the second derivative of displacements. The constitutive law is plasticity with linear hardening, defined separately for axial and bending response. We construct discrete approximation by using Hermite's polynomials, for both position vector and displacements, and present the finite element arrays and details of numerical implementation. Several numerical examples are presented in order to illustrate an excellent performance of the proposed beam model.

Keywords: Kirchhoff beam; rotated strain measure; Hermite's polynomials; elasto-plastic response

1. Introduction

Many beam models in the framework of small and large displacements have been proposed in works of Reissner (1981), Simo (1985) and Ibrahimbegovic (1995). All existing beam models can be split into two groups. The first group includes Euler-Bernoulli's models, enforcing Kirchhoff's constraint with the section that remains rigid and perpendicular to the deformed beam axis. The second group includes Reissner's type of beam model still assuming the section as rigid but no longer perpendicular to the deformed beam axis. The models in the first group neglect shear deformation and they are more suitable for representing thin structures with negligible shear deformation. The Euler-Bernoulli beam model in the framework of small displacement, yet called the classical beam theory, is well known, but an extension of this theory to the framework of large deformation/displacement is still a part of scientific research (Kitarovic 2014, Armero and Valverde 2012, Maurin *et al.* 2018). Recent works give a different formulation of such beam theory, which includes Kirchhoff's constraint, but also use an additional unphysical degree of freedom (Boyer and Primault 2004, Maassen *et al.* 2018) or Lagrange multiplier for treatment of

---

∗Corresponding author, Assistant Professor, E-mail: imamovic.ismar@gmail.com
[a]Professor
[b]Ph.D. Student

axial deformation (Meier *et al.* 2019, Meier *et al.* 2018). The second group of the geometrically exact beam models or Reissner's type of beam models, that include shear deformation, represent an extension of Timoshenko beam theory (Hadzalic *et al.* 2018, Imamovic *et al.* 2015, Hadzalic *et al.* 2018) to large deformation framework. These models were defined in classic works Reissner (1972), Simo *et al.* (1984), Ibrahimbegovic and Frey (1993a), and are later combined with many constitutive models. More recent works (Pirmanšek *et al.* 2017, Imamovic *et al.* 2017, Imamovic *et al.* 2018) present different ways of including a discontinuity in nonlinear kinematics of Reissner's beam.

The main novelty in this work concerns to the theoretical formulation and the numerical implementation of geometrically exact initially curved beam model including Kirchhoff's constraint, which is imposed in kinematic equations of Reissner's beam without the need to introduce any unphysical degree of freedom. This is achieved even for the case of constitutive law defined as plasticity with linear hardening, for both axial and bending response.

The outline of the paper is as follows. In the next section, we present theoretical formulation of kinematics, chosen constitutive law and the weak form of governing equilibrium equations. The discrete approximation and numerical implementation details are presented in Section 3. The results of several numerical simulations are given in Section 4 in order to illustrate the model performance. The main conclusions are stated in Section 5.

2. Theoretical formulation: kinematics, constitutive and weak form equilibrium equations

In the framework of large displacement gradient theory, the position vector for Reissner's beam (Ibrahimbegovic and Frey 1993) in deformed configuration can be written as

$$\boldsymbol{\varphi} := \boldsymbol{\varphi_0} + \zeta \mathbf{t} = \begin{pmatrix} x+u \\ y+v \end{pmatrix} + \zeta \begin{pmatrix} -\sin(\alpha+\psi) \\ \cos(\alpha+\psi) \end{pmatrix} \tag{1}$$

where x and y are coordinates in the reference configuration, α is initial position of cross-section, u and v are displacement components in the global coordinate system, ζ is the coordinate along the normal to the beam axis in the reference configuration and ψ is the section rotation. The corresponding form of the deformation gradient $\mathbf{F}$ (Ibrahimbegovic 2009) can be written as:

$$\mathbf{F} := \nabla \boldsymbol{\varphi} = \underbrace{\begin{bmatrix} \dfrac{dx}{ds}+\dfrac{du}{ds} & 0 \\ \dfrac{dy}{ds}+\dfrac{dv}{ds} & 0 \end{bmatrix}}_{\mathbf{F}_{u,v}=\nabla\mathbf{x}+\nabla\mathbf{u}} + \underbrace{\begin{bmatrix} -\zeta\dfrac{d\psi}{ds}\cos(\alpha+\psi) & -\sin(\alpha+\psi) \\ -\zeta\dfrac{d\psi}{ds}\sin(\alpha+\psi) & \cos(\alpha+\psi) \end{bmatrix}}_{\mathbf{F}_{\psi}=\mathbf{I}+\nabla\boldsymbol{\psi}} \tag{2}$$

where s is the coordinate along the beam axis in the reference configuration.

By using the polar decomposition of the deformation gradient $\mathbf{F}$, to attach its multiplicative split into rotation $\mathbf{R}$ and stretch $\mathbf{U}$, we can define the corresponding rotated strain measure $\mathbf{H}$:

$$\mathbf{F} = \mathbf{RU} \rightarrow \mathbf{U} = \mathbf{R}^T\mathbf{F}, \ \mathbf{R} = \begin{bmatrix} \cos(\alpha+\psi) & -\sin(\alpha+\psi) \\ \sin(\alpha+\psi) & \cos(\alpha+\psi) \end{bmatrix} \rightarrow \mathbf{H} = \mathbf{U}-\mathbf{I} \tag{3}$$

Furthermore, the stretch $\mathbf{U}$ can be additively decomposed into strech $\mathbf{U}_{u,v}$ related to displacement and strech $\mathbf{U}_\psi$ related to rotation:

$$\mathbf{U} = \mathbf{U}_{u,v} + \mathbf{U}_{\psi} \tag{4}$$

where

$$\mathbf{U}_{u,v} = \begin{bmatrix} \left(\dfrac{dx}{ds}+\dfrac{du}{ds}\right)\cos(\alpha+\psi)+\left(\dfrac{dy}{ds}+\dfrac{dv}{ds}\right)\sin(\alpha+\psi) & 0 \\ -\left(\dfrac{dx}{ds}+\dfrac{du}{ds}\right)\sin(\alpha+\psi)+\left(\dfrac{dy}{ds}+\dfrac{dv}{ds}\right)\cos(\alpha+\psi) & 0 \end{bmatrix} ; \mathbf{U}_{\psi} = \begin{bmatrix} -\zeta\dfrac{d\psi}{dx} & 0 \\ 0 & 1 \end{bmatrix} ; \mathbf{I} = \begin{bmatrix} 1 & 0 \\ 0 & 1 \end{bmatrix}$$

The rotated strain measure components can be written as

$$\Sigma = H_{11} - \zeta K = \left(\frac{dx}{ds}+\frac{du}{ds}\right)\cos\left(\alpha+\psi\right)+\left(\frac{dx}{ds}+\frac{dv}{ds}\right)\sin\left(\alpha+\psi\right)-1$$

$$\Gamma = H_{21} = -\left(\frac{dx}{ds}+\frac{du}{ds}\right)\sin\left(\alpha+\psi\right)+\left(\frac{dx}{ds}+\frac{dv}{ds}\right)\cos\left(\alpha+\psi\right) \tag{5}$$

$$K = \frac{d\psi}{ds}$$

where Σ, Γ are, respectively, the axial and shear strain in rotated configuration and K is the curvature strain.

The results in Eqs. (5)$_1$ and (5)$_2$ can be rewritten in compact matrix notation as:

$$\boldsymbol{\Sigma} = (\Sigma,\Gamma)^T = \boldsymbol{\Lambda}_0^T \boldsymbol{\Lambda}^T \left(\mathbf{h}(\mathbf{a}) - \boldsymbol{\Lambda}\boldsymbol{\Lambda}_0\right) \tag{6}$$

$$\boldsymbol{\Lambda}_0 = \begin{bmatrix} \cos\alpha & -\sin\alpha \\ \sin\alpha & \cos\alpha \end{bmatrix} ; \boldsymbol{\Lambda} = \begin{bmatrix} \cos\psi & -\sin\psi \\ \sin\psi & \cos\psi \end{bmatrix} ; \mathbf{h}(\mathbf{a}) = \begin{pmatrix} \dfrac{dx}{ds}+\dfrac{du}{ds} \\ \dfrac{dy}{ds}+\dfrac{dv}{ds} \end{pmatrix}$$

By imposing at this stage Kirchhoff's constraint, implying that the beam section remains not only plane, but also perpendicular to the beam axis resulting with zero shear strain ($\Gamma=0$), we further obtain

$$\tan(\alpha+\psi) = \frac{\dfrac{dy}{ds}+\dfrac{dv}{ds}}{\dfrac{dx}{ds}+\dfrac{du}{ds}} => \tilde{\psi} = \arctan\left(\frac{\dfrac{dy}{ds}+\dfrac{dv}{ds}}{\dfrac{dx}{ds}+\dfrac{du}{ds}}\right) - \alpha \tag{7}$$

With vanished shear deformation, Eq. (6) can be rewritten as

$$\boldsymbol{\Sigma} = (\Sigma,\Gamma=0)^T = \boldsymbol{\Lambda}_0^T \tilde{\boldsymbol{\Lambda}}^T \left(\mathbf{h}(\mathbf{a}) - \tilde{\boldsymbol{\Lambda}}\boldsymbol{\Lambda}_0\right) ; \tilde{\boldsymbol{\Lambda}} = \begin{bmatrix} \cos\tilde{\psi} & -\sin\tilde{\psi} \\ \sin\tilde{\psi} & \cos\tilde{\psi} \end{bmatrix} \tag{8}$$

By exploiting the result in (7) and in (5)$_3$ we can obtain the corresponding expression for curvature of the geometrically exact Kirchhoff beam

$$
\begin{aligned}
K = \frac{d\tilde{\psi}}{ds} &= \frac{-\left(\dfrac{d^2x}{ds^2}+\dfrac{d^2u}{ds^2}\right)\left(\dfrac{dy}{ds}+\dfrac{dv}{ds}\right)+\left(\dfrac{d^2y}{ds^2}+\dfrac{d^2v}{ds^2}\right)\left(\dfrac{dx}{ds}+\dfrac{du}{ds}\right)}{\left(\dfrac{dx}{ds}+\dfrac{du}{ds}\right)^2+\left(\dfrac{dy}{ds}+\dfrac{dv}{ds}\right)^2} - \frac{d\alpha}{ds} = \\
&= \left(\left(\frac{d^2y}{ds^2}+\frac{d^2v}{ds^2}\right)\cos(\alpha+\tilde{\psi})-\left(\frac{d^2x}{ds^2}+\frac{d^2u}{ds^2}\right)\sin(\alpha+\tilde{\psi})\right)\frac{1}{\Delta l} - \frac{d\alpha}{ds} = \\
&= \boldsymbol{\Lambda}_0\frac{d\tilde{\boldsymbol{\Lambda}}^T}{d\tilde{\psi}}\frac{d\mathbf{h}(\mathbf{a})}{ds}\frac{1}{\Delta l} - \frac{d\alpha}{ds}
\end{aligned} \tag{9}
$$

where

$$\frac{d\tilde{\mathbf{\Lambda}}^T}{d\tilde{\psi}} = \begin{pmatrix} -\sin\tilde{\psi} & \cos\tilde{\psi} \end{pmatrix}^T; \frac{d\mathbf{h}(\mathbf{a})}{ds} = \begin{pmatrix} \dfrac{d^2x}{ds^2} + \dfrac{d^2u}{ds^2} \\[2mm] \dfrac{d^2y}{ds^2} + \dfrac{d^2v}{ds^2} \end{pmatrix}; \Delta l = \sqrt{\left(\frac{dx}{ds} + \frac{du}{ds}\right)^2 + \left(\frac{dy}{ds} + \frac{dv}{ds}\right)^2}$$

In the elastic regime the simplest set of the constitutive equations for finite strain beam is chosen in terms of Biot's stress resultants and rotated strain measure:

$$\mathbf{T} = \mathbf{C}^e \mathbf{H}; \ \mathbf{C}^e = diag\left(EA, EI\right) \tag{10}$$

By using the rotated strain measure $\mathbf{H}$, we obtain the only non-zero components, defined as:

$$H_{11} = \Sigma - \zeta K \tag{11}$$

The weak form of the equilibrium equation, see (Ibrahimbegovic and Frey 1993a):

$$G\left(\mathbf{a}, \hat{\mathbf{a}}\right) := \int_L \left(\hat{\Sigma} N + \hat{K} M\right) dx - G^{ext} = 0 \tag{12}$$

In Eq. (12) above, N and M denote stress resultants, expressed in terms of the Biot's stress:

$$\mathbf{T} = \left(N, M\right)^T; \ N = \int_A T^{11} dA = EA\Sigma; \ M = -\int_A \zeta T^{11} dA = EIK \tag{13}$$

The virtual strain measure can be derived by taking the directional derivative of the strain measures (8), which can be written explicitly as:

$$\hat{\Sigma} = \frac{d\hat{u}}{ds}\cos\left(\alpha + \tilde{\psi}\right) + \frac{d\hat{v}}{ds}\sin\left(\alpha + \tilde{\psi}\right) +$$

$$+ \hat{\psi}\underbrace{\left[-\left(\frac{dx}{ds} + \frac{du}{ds}\right)\sin\left(\alpha + \tilde{\psi}\right) + \left(\frac{dy}{ds} + \frac{dv}{ds}\right)\cos\left(\alpha + \tilde{\psi}\right)\right]}_{=\Gamma=0} = \mathbf{\Lambda}_0^T \tilde{\mathbf{\Lambda}}^T \mathbf{d}(\hat{\mathbf{a}}) \tag{14}$$

$$\hat{K} = \left(-\frac{d^2\hat{u}}{ds^2}\sin\left(\alpha + \tilde{\psi}\right) + \frac{d^2\hat{v}}{ds^2}\cos\left(\alpha + \tilde{\psi}\right)\right)\frac{1}{\Delta l} -$$

$$- \hat{\psi}\left(\left(\frac{d^2x}{ds^2} + \frac{d^2u}{ds^2}\right)\cos\left(\alpha + \tilde{\psi}\right) + \left(\frac{d^2y}{ds^2} + \frac{d^2v}{ds^2}\right)\sin\left(\alpha + \tilde{\psi}\right)\right)\frac{1}{\Delta l} = \tag{15}$$

$$= \mathbf{\Lambda}_0^T \frac{d\tilde{\mathbf{\Lambda}}^T}{d\tilde{\psi}}\frac{d\mathbf{d}(\hat{\mathbf{a}})}{ds}\frac{1}{\Delta l} - \hat{\psi}\mathbf{\Lambda}_0^T \tilde{\mathbf{\Lambda}}^T \frac{d\mathbf{h}(\mathbf{a})}{ds}\frac{1}{\Delta l}; \frac{d\mathbf{d}(\hat{\mathbf{a}})^T}{ds} = \left(\frac{d^2\hat{u}}{ds^2} \quad \frac{d^2\hat{v}}{ds^2}\right)^T$$

The virtual rotation can be expressed in terms of first derivatives of virtual displacement field:

$$\hat{\psi} = \frac{d}{d\beta}\left(\tilde{\psi}(\mathbf{a} + \beta\hat{\mathbf{a}})\right) = \left(-\frac{d\hat{u}}{ds}\sin\left(\alpha + \tilde{\psi}\right) + \frac{d\hat{v}}{ds}\cos\left(\alpha + \tilde{\psi}\right)\right)\frac{1}{\Delta l} = \mathbf{\Lambda}_0^T \frac{d\tilde{\mathbf{\Lambda}}^T}{d\tilde{\psi}}\mathbf{d}(\hat{\mathbf{a}})\frac{1}{\Delta l} \tag{16}$$

Finally, with previous results in hand, we can express virtual curvature as

$$\hat{K} = \mathbf{\Lambda}_0^T \frac{d\tilde{\mathbf{\Lambda}}^T}{d\tilde{\psi}}\frac{d\mathbf{d}(\hat{\mathbf{a}})}{ds}\frac{1}{\Delta l} - \mathbf{\Lambda}_0^T \frac{d\tilde{\mathbf{\Lambda}}^T}{d\tilde{\psi}}\mathbf{d}(\hat{\mathbf{a}})\mathbf{\Lambda}_0^T \tilde{\mathbf{\Lambda}}^T \frac{d\mathbf{h}(\mathbf{a})}{ds}\frac{1}{\Delta l^2} \tag{17}$$

By using previous results Eqs. (8), (14), (9) and (17), the final expression of the equilibrium

equation weak form Eq. (12), can be written as

$$G(\mathbf{a},\hat{\mathbf{a}}) := \int_L \left(\mathbf{d}(\hat{\mathbf{a}})^T \tilde{\mathbf{\Lambda}} \mathbf{\Lambda}_0 \right) EA \left(\mathbf{\Lambda}_0^T \tilde{\mathbf{\Lambda}}^T \left(\mathbf{h}(\mathbf{a}) - \mathbf{\Lambda}_0 \tilde{\mathbf{\Lambda}} \right) \right) dx +$$

$$+ \int_L \left(\left(\frac{d\mathbf{d}(\hat{\mathbf{a}})^T}{ds} \frac{d\tilde{\mathbf{\Lambda}}}{d\tilde{\psi}} \mathbf{\Lambda}_0 \frac{1}{\Delta l} - \mathbf{d}(\hat{\mathbf{a}}) \frac{d\tilde{\mathbf{\Lambda}}}{d\tilde{\psi}} \mathbf{\Lambda}_0 \mathbf{\Lambda}_0^T \tilde{\mathbf{\Lambda}}^T \frac{d\mathbf{h}(\mathbf{a})}{ds} \frac{1}{\Delta l^2}(\ ) \right) EI \left(\mathbf{\Lambda}_0^T \frac{d\tilde{\mathbf{\Lambda}}^T}{d\tilde{\psi}} \frac{d\mathbf{h}(\mathbf{a})}{ds} \frac{1}{\Delta l} \right) \right) dx - \tag{18}$$

$$- G^{ext} = 0$$

The final step needed for numerical implementation is the linearization of the weak form of equilibrium equations so that an iterative strategy can be employed. In order to provide quadratic convergence and employ Newton's method, we need to find the consistent tangent stiffness. It can be obtained by the consistent linearization of the expression (18) to get

$$L(G)\big|_{\mathbf{a}} = G(\mathbf{a},\hat{\mathbf{a}})\big|_{\mathbf{a}} + \frac{d}{d\beta}\Big[G(\hat{\mathbf{a}}, \mathbf{a} + \beta\Delta\mathbf{a}) \Big]\bigg|_{\beta}$$

$$= G(\mathbf{a},\hat{\mathbf{a}}) + \int_L \left(\mathbf{d}(\hat{\mathbf{a}}), \frac{d\mathbf{d}(\hat{\mathbf{a}})}{ds} \right)^T \left[\mathbf{D}^\Sigma + \mathbf{D}^K \right] \begin{pmatrix} \mathbf{d}(\Delta\mathbf{a}) \\ \dfrac{d\mathbf{d}(\Delta\mathbf{a})}{ds} \end{pmatrix} ds \tag{19}$$

where $\mathbf{D}^\Sigma$ and $\mathbf{D}^\Sigma$ are tangent stiffness's related to axial and bending response, which can be decomposed into material $\mathbf{D}_m^{\Sigma,K}$ and geometric $\mathbf{D}_g^{\Sigma,K}$ part:

$$\mathbf{D}^\Sigma = \underbrace{\mathbf{\Lambda}_0 \tilde{\mathbf{\Lambda}} EA \tilde{\mathbf{\Lambda}}^T \mathbf{\Lambda}_0^T}_{\mathbf{D}_m^\Sigma} + \underbrace{\mathbf{\Lambda}_0 \frac{d\tilde{\mathbf{\Lambda}}}{d\tilde{\psi}} \frac{N}{\Delta l} \frac{d\tilde{\mathbf{\Lambda}}^T}{d\tilde{\psi}} \mathbf{\Lambda}_0^T}_{\mathbf{D}_g^\Sigma} \tag{20}$$

The second part of tangent stiffness related to bending response can be written as:

$$\mathbf{D}^K = \mathbf{D}_m^K + \mathbf{D}_g^K; \quad \mathbf{D}_m^K = \begin{bmatrix} \mathbf{D}_{m,11}^K & \mathbf{D}_{m,12}^K \\ \mathbf{D}_{m,21}^K & \mathbf{D}_{m,22}^K \end{bmatrix}; \quad \mathbf{D}_g^K = \begin{bmatrix} \mathbf{D}_{g,11}^K & \mathbf{D}_{g,12}^K \\ \mathbf{D}_{g,21}^K & \mathbf{D}_{g,22}^K \end{bmatrix} \tag{21}$$

where

$$\mathbf{D}_{m,11}^K = \mathbf{\Lambda}_0 \frac{d\tilde{\mathbf{\Lambda}}}{d\tilde{\psi}} \frac{d\mathbf{h}(\mathbf{a})^T}{ds} \mathbf{\Lambda}_0 \frac{d^2\tilde{\mathbf{\Lambda}}}{d\tilde{\psi}^2} \frac{d^2\tilde{\mathbf{\Lambda}}^T}{d\tilde{\psi}^2} \mathbf{\Lambda}_0^T \frac{d\mathbf{h}(\mathbf{a})}{ds} \frac{d\tilde{\mathbf{\Lambda}}^T}{d\tilde{\psi}} \mathbf{\Lambda}_0^T \frac{1}{\Delta l^4} EI;$$

$$\mathbf{D}_{g,11}^K = \mathbf{\Lambda}_0 \frac{d\tilde{\mathbf{\Lambda}}}{d\tilde{\psi}} \frac{d\mathbf{h}(\mathbf{a})^T}{ds} \mathbf{\Lambda}_0 \frac{d^2\tilde{\mathbf{\Lambda}}}{d\tilde{\psi}^2} \frac{d\tilde{\mathbf{\Lambda}}^T}{d\tilde{\psi}} \mathbf{\Lambda}_0^T \frac{M}{\Delta l^3};$$

$$\mathbf{D}_{m,12}^K = \mathbf{\Lambda}_0 \frac{d\tilde{\mathbf{\Lambda}}}{d\tilde{\psi}} \frac{d\mathbf{h}(\mathbf{a})^T}{ds} \mathbf{\Lambda}_0 \frac{d^2\tilde{\mathbf{\Lambda}}}{d\tilde{\psi}^2} \frac{d\tilde{\mathbf{\Lambda}}^T}{d\tilde{\psi}} \mathbf{\Lambda}_0^T \frac{EI}{\Delta l^3};$$

$$\mathbf{D}_{g,12}^K = \mathbf{\Lambda}_0 \frac{d\tilde{\mathbf{\Lambda}}}{d\tilde{\psi}} \frac{d^2\tilde{\mathbf{\Lambda}}^T}{d\tilde{\psi}^2} \mathbf{\Lambda}_0^T \frac{M}{\Delta l^2};$$

$$\mathbf{D}_{m,21}^K = \mathbf{\Lambda}_0 \frac{d\tilde{\mathbf{\Lambda}}}{d\tilde{\psi}} \frac{d\tilde{\mathbf{\Lambda}}^T}{d\tilde{\psi}} \mathbf{\Lambda}_0^T \frac{d\mathbf{h}(\mathbf{a})}{ds} \frac{d\tilde{\mathbf{\Lambda}}^T}{d\tilde{\psi}} \mathbf{\Lambda}_0^T \frac{EI}{\Delta l^3};$$

$$\mathbf{D}_{g,21}^K = \mathbf{\Lambda}_0 \frac{d^2\tilde{\mathbf{\Lambda}}}{d\tilde{\psi}^2} \frac{d\tilde{\mathbf{\Lambda}}^T}{d\tilde{\psi}} \mathbf{\Lambda}_0^T \frac{M}{\Delta l^2};$$

$$\mathbf{D}_{m,22}^K = \mathbf{\Lambda}_0 \frac{d\tilde{\mathbf{\Lambda}}}{d\tilde{\psi}} \frac{d\tilde{\mathbf{\Lambda}}^T}{d\tilde{\psi}} \mathbf{\Lambda}_0^T \frac{EI}{\Delta l^2};$$

In the elastic regime we choose the simplest set of linear constitutive equations for finite strain beam in terms of Biot's stress resultants and rotated strain measure, see (10). In the plastic regime, the same constitutive relation can be used by using elastoplastic modulus C^{ep} instead of elastic modulus C^e. The next step is the additive decomposition of the displacement and rotation gradients into elastic part $(\bullet^e)$ and plastic part $(\bullet^p)$, which corresponds to multiplicative decomposition of deformation gradient:

$$\mathbf{F} = \mathbf{I} + \nabla \mathbf{u}^e + \nabla \mathbf{u}^p + \mathbf{I} + \nabla \tilde{\psi}^e + \nabla \tilde{\psi}^p =$$

$$= \left(\nabla \mathbf{x} + \nabla \mathbf{u}^e \right) \left(\mathbf{I} + \frac{\nabla \mathbf{u}^p}{\nabla \mathbf{x} + \nabla \mathbf{u}^e} \right) + \left(\mathbf{I} + \nabla \tilde{\psi}^e \right) \left(\mathbf{I} + \frac{\nabla \tilde{\psi}^p}{\mathbf{I} + \nabla \tilde{\psi}^e} \right) = \mathbf{F}^e_{u,v} \mathbf{F}^p_{u,v} + \mathbf{F}^e_\psi \mathbf{F}^p_\psi \tag{22}$$

We also note that such multiplicative decomposition of the deformation gradient leads to the additive decomposition of the stretch tensor $\mathbf{U}$ (Imamovic *et al.* 2017):

$$\mathbf{U} = \mathbf{R}^{\mathbf{T}} \left(\nabla \mathbf{x} + \nabla \mathbf{u}^e + \nabla \mathbf{u}^p \right) + \mathbf{R}^{\mathbf{T}} \left(\mathbf{I} + \nabla \tilde{\psi}^e + \nabla \tilde{\psi}^p \right) = \underbrace{\mathbf{U}^e_{u,v} + \mathbf{U}^p_{u,v}}_{\mathbf{U}_{u,v}} + \underbrace{\mathbf{U}^e_\psi + \mathbf{U}^p_\psi}_{\mathbf{U}_\psi} \tag{23}$$

where:

$$\mathbf{U}^e_{u,v} = \begin{bmatrix} \left(\dfrac{dx}{ds} + \dfrac{du^e}{ds} \right)\cos(\alpha + \tilde{\psi}) + \left(\dfrac{dx}{ds} + \dfrac{dv}{ds} \right)\sin(\alpha + \tilde{\psi}) & 0 \\ -\left(\dfrac{dx}{ds} + \dfrac{du^e}{ds} \right)\sin(\alpha + \tilde{\psi}) + \left(\dfrac{dx}{ds} + \dfrac{dv}{ds} \right)\cos(\alpha + \tilde{\psi}) & 0 \end{bmatrix}; \mathbf{U}^e_\psi = \begin{bmatrix} -\zeta\dfrac{d\tilde{\psi}^e}{ds} & 0 \\ 0 & 1 \end{bmatrix}$$

$$\mathbf{U}^p_{u,v} = \begin{bmatrix} \dfrac{du^p}{ds}\cos(\alpha + \tilde{\psi}) + \dfrac{dv^p}{ds}\sin(\alpha + \tilde{\psi}) & 0 \\ -\dfrac{du^p}{ds}\sin(\alpha + \tilde{\psi}) + \dfrac{dv^p}{ds}\cos(\alpha + \tilde{\psi}) & 0 \end{bmatrix}; \mathbf{U}^p_\psi = \begin{bmatrix} -\zeta\dfrac{d\tilde{\psi}^p}{ds} & 0 \\ 0 & 0 \end{bmatrix}$$

The Helmholtz free energy can be defined as a quadratic form:

$$\Psi(\mathbf{U}^e, \xi^p) = \underbrace{\frac{1}{2}\mathbf{U}^{e,T} \cdot \mathbf{C}^e \cdot \mathbf{U}^e}_{\Psi^e} + \underbrace{\frac{1}{2}\xi^{p,T} \cdot \mathbf{K}^h \cdot \xi^p}_{\Xi^p} \tag{24}$$

where $\mathbf{U}^e$ is the elastic part of the stretch tensor, ξ^p is the vector of hardening variables and $\mathbf{K}^h$ are the corresponding hardening moduli. The yield criterion condition is composed of two uncoupled criteria. The first is related to the axial force and the second to the bending moment. Both criteria are postulated in terms of stress resultants of the Biot stress, imposing that

$$\bar{\phi}(\mathbf{T}, \bar{\mathbf{q}}) \leq \mathbf{T} - \left(\mathbf{T}_y - \mathbf{q} \right) \tag{25}$$

where: $\mathbf{q} = [q^N, q^M]$ is the vector of internal hardening stress like variables related to the axial force and bending moment, respectively; and $\mathbf{T}_y = [N_y, M_y]$ are the yield stress resultants of Biot stress, axial force and bending moment. The second principle of thermodynamics (Ibrahimbegovic 2009) can be used for state that the plastic dissipation must remain non-negative:

$$0 \leq \mathcal{D} = \underbrace{\left(\mathbf{T} - \frac{d\Psi^e}{d\mathbf{U}^e} \right)\dot{\mathbf{U}}^e}_{\mathcal{D}^e = 0} + \underbrace{\mathbf{T}\dot{\mathbf{U}}^p - \frac{\partial \Xi^p}{\partial \xi^p}\frac{d\xi^p}{dt}}_{\mathcal{D}^p} \tag{26}$$

The principle of maximum plastic dissipation (Hill 1950) can then be enforced to obtain the corresponding evolution equations of plastic strain and hardening variable. This principle can be formulated as the constrained minimization problem, where the constraint is yield function in (25). This can further be recast as corresponding unconstrained minimization by using the Lagrange multiplier method:

$$\min_{\mathbf{T},\mathbf{q}} \max_{\dot{\gamma}} \left[L^p(\mathbf{T},\mathbf{q},\dot{\gamma}) = -\mathscr{D}^p(\mathbf{T},\mathbf{q}) + \dot{\gamma} \cdot \phi(\mathbf{T},\mathbf{q}) \right] \tag{27}$$

where $\dot{\gamma}$ is plastic multiplier. The corresponding Kuhn-Tucker optimality conditions result with the evolution equations for internal variables in rate form, along with the loading/unloading conditions:

$$\frac{\partial \bar{L}^p}{\partial \mathbf{T}} = -\dot{\bar{\mathbf{U}}}^p + \dot{\bar{\gamma}} \frac{\partial \bar{\phi}}{\partial \mathbf{T}} = 0 \Rightarrow \dot{\bar{\mathbf{U}}}^p = \dot{\bar{\gamma}} \frac{\partial \bar{\phi}}{\partial \mathbf{T}}$$

$$\frac{\partial \bar{L}^p}{\partial \bar{\mathbf{q}}} = -\frac{\partial \bar{\xi}^p}{\partial t} + \dot{\bar{\gamma}} \frac{\partial \bar{\phi}}{\partial \bar{\mathbf{q}}} = 0 \Rightarrow \frac{\partial \bar{\xi}^p}{\partial t} = \dot{\bar{\gamma}} \frac{\partial \bar{\phi}}{\partial \bar{\mathbf{q}}} \tag{28}$$

$$\dot{\bar{\gamma}} \geq 0, \quad \bar{\phi} \leq 0, \quad \dot{\bar{\gamma}}\bar{\phi} = 0$$

The appropriate value of plastic multiplier $\dot{\gamma}$ can be determined from the plastic consistency condition for the case of sustained plastic flow:

$$\dot{\phi} = 0 \Rightarrow \dot{\gamma} = \frac{\frac{\partial \phi}{\partial \mathbf{T}} \mathbf{C}^e \dot{\mathbf{U}}}{\frac{\partial \phi}{\partial \mathbf{T}} \mathbf{C}^e \frac{\partial \phi}{\partial \mathbf{T}} + \frac{\partial \phi}{\partial \mathbf{q}} \mathbf{K}^h \frac{\partial \phi}{\partial \mathbf{q}}}; \quad \mathbf{C}^e = \begin{bmatrix} EA & 0 \\ 0 & EI \end{bmatrix} \tag{29}$$

By replacing the last result in stress rate equation, we can obtain the elasto-plastic modulus $\mathbf{C}^{ep}$ that should replace the elastic modulus $\mathbf{C}^e$ in plastic regime:

$$C^{ep} = \mathbf{C}^e - \frac{\mathbf{C}^e \frac{\partial \phi}{\partial \mathbf{T}} \otimes \mathbf{C}^e \frac{\partial \phi}{\partial \mathbf{T}}}{\frac{\partial \phi}{\partial \mathbf{T}} \mathbf{C}^e \frac{\partial \phi}{\partial \mathbf{T}} + \frac{\partial \phi}{\partial \mathbf{q}} \mathbf{K}^h \frac{\partial \phi}{\partial \mathbf{q}}} \tag{30}$$

We note in passing that the elasto-plastic tangent modulus above remains the same in the time-discretized problem, which is obtained by using the backward Euler time integration scheme applied to (28) with result replaced in (19).

3. Finite element approximation

We choose the Hermite's polynomials (Meier *et al.* 2019, Sonneville *et al.* 2017) for constructing discrete approximation of bot position vector (x and y) and displacements (u and v). Some details of such numerical implementation are here illustrated for a beam element with two nodes, with position vectors in the initial and deformed configuration can be written as:

$$\mathbf{x}^h(\xi) = \sum_{a=1}^{2} N_a^u(\xi) \mathbf{x}_a^0 + \frac{c}{2} \sum_{a=1}^{2} N_a^\alpha(\xi) \mathbf{t}_{0,a}; \quad \mathbf{t}_{0,a}^T = (\cos\alpha, \sin\alpha)^T$$

$$\boldsymbol{\varphi}^h(\xi) = \sum_{a=1}^{2} N_a^u(\xi)(\mathbf{x}_a^0 + \mathbf{u}_a) + \frac{c}{2} \sum_{a=1}^{2} N_a^\alpha(\xi) \mathbf{t}_a; \quad \mathbf{t}_a^T = (\cos(\alpha+\tilde{\psi}), \sin(\alpha+\tilde{\psi}))^T \tag{31}$$

where $\mathbf{X}^0_a$ is a position vector in the initial configuration, $\mathbf{t}_{0,a}$ is a vector of tangents to initial predefined configuration, $\mathbf{u}_a$ is a nodal displacement vector, $\mathbf{t}^T_a$ is a vector of tangents in reference configuration and c is a constant equal to length of beam element.

The derivatives of Eq. (31), needed for approximation of proposed beam model, can be written in explicit form as:

$$\frac{d}{d\xi}x^h(\xi) = \sum_{a=1}^{2}\frac{d}{d\xi}N_a^u(\xi)x_a; \frac{d^2}{d\xi^2}x^h(\xi) = \sum_{a=1}^{2}\frac{d^2}{d\xi^2}N_a^u(\xi)x_a - \frac{c}{2}\sin(\alpha)\sum_{a=1}^{2}\frac{d^2}{d\xi^2}N_a^\psi(\xi)\alpha_a;$$

$$\frac{d}{d\xi}y^h(\xi) = \sum_{a=1}^{2}\frac{d}{d\xi}N_a^v(\xi)y_a; \frac{d^2}{d\xi^2}y^h(\xi) = \sum_{a=1}^{2}\frac{d^2}{d\xi^2}N_a^v(\xi)y_a + \frac{c}{2}\cos(\alpha)\sum_{a=1}^{2}\frac{d^2}{d\xi^2}N_a^\psi(\xi)\alpha_a;$$

$$\frac{d}{d\xi}\varphi_x^h(\xi) = \sum_{a=1}^{2}\frac{d}{d\xi}N_a^u(\xi)(x_a+u_a); \frac{d}{d\xi}\varphi_y^h(\xi) = \sum_{a=1}^{2}\frac{d}{d\xi}N_a^v(\xi)(y_a+v_a) \qquad (32)$$

$$\frac{d^2}{d\xi^2}\varphi_x^h(\xi) = \sum_{a=1}^{2}\frac{d^2}{d\xi^2}N_a^u(\xi)(x_a+u_a) - \frac{c}{2}\sin(\alpha+\tilde{\psi})\sum_{a=1}^{2}\frac{d^2}{d\xi^2}N_a^\psi(\xi)(\alpha_a+\psi_a);$$

$$\frac{d^2}{d\xi^2}\varphi_y^h(\xi) = \sum_{a=1}^{2}\frac{d^2}{d\xi^2}N_a^v(\xi)(y_a+v_a) + \frac{c}{2}\cos(\alpha+\tilde{\psi})\sum_{a=1}^{2}\frac{d^2}{d\xi^2}N_a^\psi(\xi)(\alpha_a+\psi_a);$$

where

$$N_1^u(\xi) = \left(\xi^3 - 3\xi + 2\right)/4; \qquad N_2^u(\xi) = \left(-\xi^3 + 3\xi + 2\right)/4;$$

$$N_1^v(\xi) = \left(\xi^3 - 3\xi + 2\right)/4; \qquad N_2^v(\xi) = \left(-\xi^3 + 3\xi + 2\right)/4;$$

$$N_1^\psi(\xi) = \left(\xi^3 - \xi^2 - \xi + 1\right)/4; \quad N_2^\psi(\xi) = \left(\xi^3 + \xi^2 - \xi - 1\right)/4;$$

and mapping of domena $s \in [0, L]$ to $\xi \in [-1,1]$

$$x = (1-\xi)\,x_1/2 + (1+\xi)\,x_2/2 \Rightarrow x = (x_1+x_2)/2 + (x_2-x_1)\xi/2$$
$$y = (1-\xi)\,y_1/2 + (1+\xi)\,y_2/2 \Rightarrow y = (y_1+y_2)/2 + (y_2-y_1)\xi/2 \Rightarrow$$

$$\Rightarrow j(\xi) = \frac{ds}{d\xi} = \sqrt{\left(\frac{dx}{d\xi}\right)^2 + \left(\frac{dy}{d\xi}\right)^2}$$

4. Numerical examples

Several numerical examples are presented in this section in order to illustrate the performance of the proposed finite element formulation. All numerical computations are performed with a research version of the computer program FEAP (Taylor 2008). The proposed model is implemented and computed results are compared with those obtained by using FEAP built-in Reissner beam developed by Ibrahimbegovic.

4.1 Straight cantilever under imposed end rotation

In this example we present two different types of a response for a cantilever beam under free-end bending load. The geometric properties of the cross section correspond to standard hot rolled *IPE 200* section and material properties take values for steel class *S235*. The initially straight cantilever beam model is constructed with three different meshes of 2, 4 and 8 elements. Each analysis is performed under imposed end rotation $\psi = 2\pi$. The first analysis represents the linear elastic response (see Fig. 1(a)), the second analysis represents the elasto-plastic response that
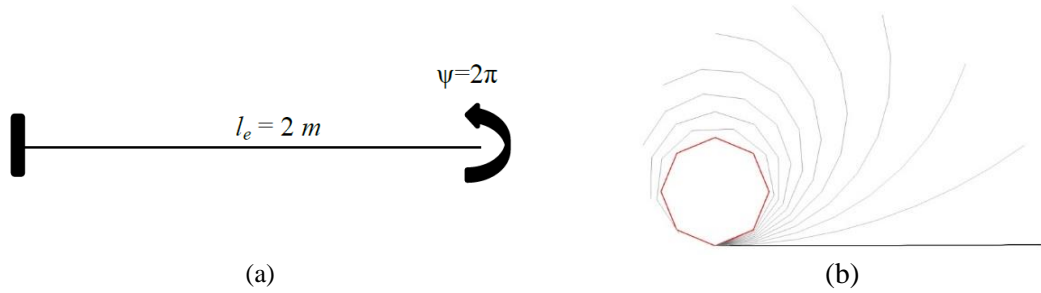
Fig. 1 Straight cantilever beam: geometry and deformed configurations
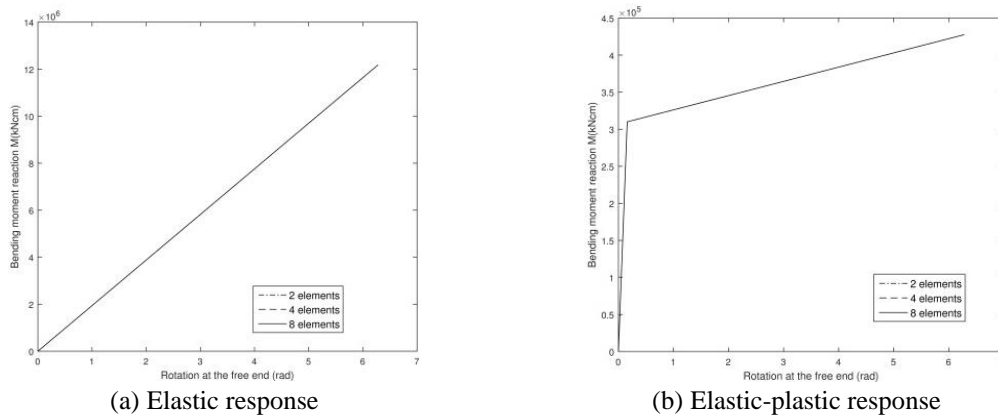
Fig. 2 Responses of the straight cantilever beam

Table 1 Cantilever beam under imposed an end rotation

No. of elements	Bending moment	
	Elastic analysis	Elastoplastic anal.
2	1218300 kNcm	427560 kNcm
4	1218300 kNcm	427560 kNcm
8	1218300 kNcm	427560 kNcm
16	1218300 kNcm	427560 kNcm
Exact	1218320 kNcm	427556.43 kNcm
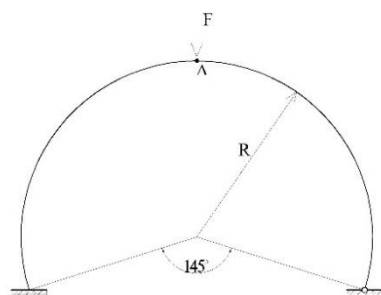
Constitutive parameters:
$EI = 10^6$
$EA = 100\, EI$
$R = 100$

Corresponding rectangular cross-section:
$b = 1.437$ (width)
$h = 0.346$ (height)

Plasticity (assumed):
$K_{hb} = K_{ha} = 10^6$
$M_y = 11468.8$ (yield bending moment)
$N_y = 198881$ (yield axial force)
$\sigma_y = 400000$ (yield stress)

Fig. 3 Clamped-hinged circular arc: geometry and constitutive parameters

reaches hardening phase (see Fig. 2(b)). The response diagrams show that the proposed model can provide mesh independent response.

For the chosen properties of the cantilever (Young's modulus: $E=2\cdot104$ kN/cm^2; hardening modulus: $K=0.05E$; moment of inertia: $I=1940$ cm^4; area of the cross section: $A=28.5$ cm^2; yield bending moment: $M_y=310000$ $kNcm$). Some of the results can be verified analytically. Namely, the elastic bending moment can be computed as $M_e=\pi\cdot EI/L=1218320$ $kNcm$ and the elasto-plastic bending moment as $M_{ep}=(\pi-K_y)\cdot EK/(E+K)L + K_y\cdot EI/L=427556.43$ $kNcm$. The comparison between these reference values against numerical results computed with different number of elements, is presented in Table 1.
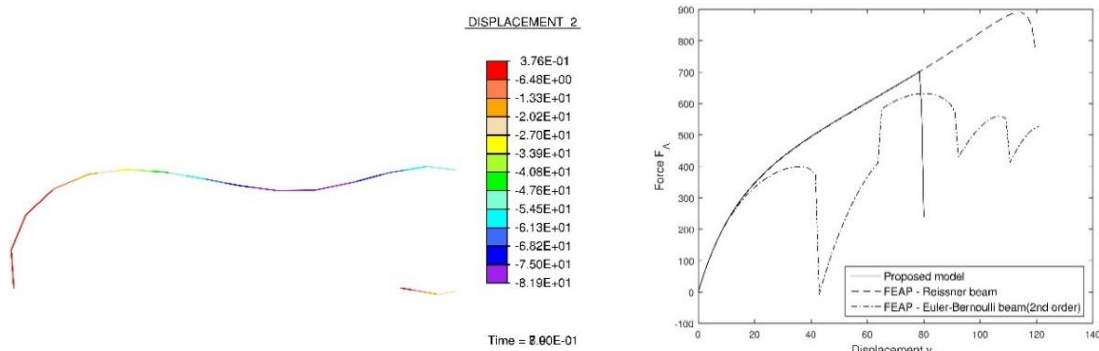
Fig. 4 Elastic analysis: deformed structure and response curve (F_A-v_A)

| (a) Plastic response | (b) Comparison proposed model vs. FEAP |
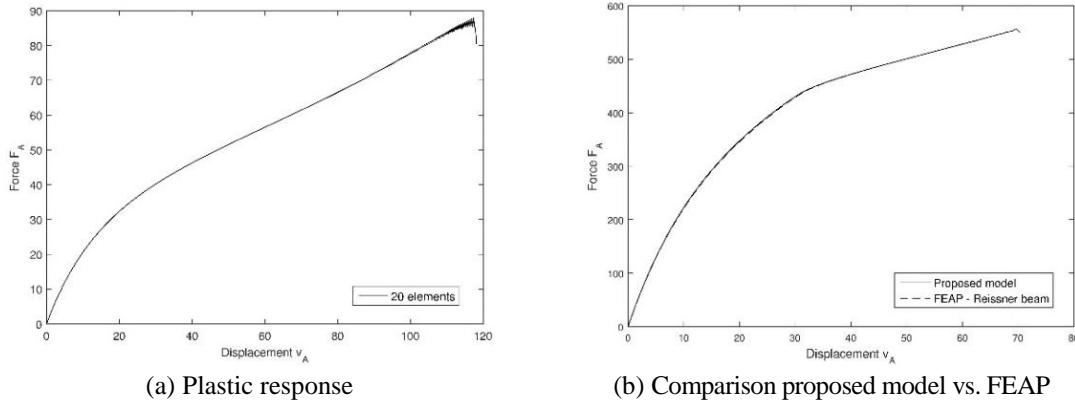
Fig. 5 Plastic analysis

Table 2 Buckling load of the circular arc

Formulation	Buckling load
Present	721
Ibrahimbegovic and Frey (1993)	897.5
DaDeppo and Schmidt (1975)	897
FEAP – Reissner's beam (multi-layered cross-section)	890.22
FEAP – Euler-Bernoulli beam (2nd order) (multi-layered cross-section)	631.9 (397.7)

4.2 Bending of deep arc

This example presents a non-linear analysis of a circular arch whose one end is clamped and the other hinged. The chosen properties for the arc are presented in Fig 3. The force is applied at the top of arc (point A), while the constitutive parameters for elastic analysis are chosen that axial modulus is being 100 times larger than bending modulus, see (Ibrahimbegovic and Frey 1993a, DaDeppo and Schmidt 1975). In order to show the performance of proposed beam model, we have also performed plastic analysis, where we assumed that hardening modulus is 10 times smaller than corresponding elastic bending modulus and the yield bending moment is equal to zero, while the axial response remains elastic. With the aim of comparing computed results, both analyses are also performed by using FEAP built-in beam models.

The linear stability analysis has determined critical force, which is smaller than the value obtained by using Reissner's beam model in Ibrahimbegovic and Frey (1993), DaDeppo and Schmidt (1975) and FEAP (Reissner's beam and Euler-Bernoulli beam (2nd order), multi-layered cross-section), see Table 2.

The pre-buckling response matches the reference response very well, but the critical point is lower and is reached under smaller structure deformation. It is known that the critical load depends on a model formulation (Fig. 4), but to the best of the authors knowledge the literature review did not reveal the reference solution of critical load for deep arc obtained by using either Kirchoff or (nonlinear) Euler Bernoulli beam. The FEAP built-in (2nd order) Euler-Bernoulli beam provides even lower critical point than the proposed beam model. However, the pre-buckling response matching with the reference solution is evident.

Two stability analyses with included plastic material behavior are performed. In the first analysis (Fig. 5(a)) we have adopted listed material properties (M_y=0, N_y=∞) (Fig. 3) in order to show the capability of the proposed model to reach large structural deformation, such is obtained in reference works. The second stability analysis is performed with both the proposed model and Reissner beam (FEAP), by using listed material properties (Fig. 3). Results are shown in Fig 5b. We can conclude that a good match between two responses is obtained. We can also conclude that the proposed model allows to capture larger structural deformation compared to FEAP built-in Reissner beam.

4.3 Williams toggle frame

In this example, we present the capability of the presented beam model to predict the response of a shallow arc, including buckling effect. In order to validate obtained results, geometry and material properties (Fig. 6) are set according to classic work Williams (1964). The linear elastic computation of shallow beam/arc is performed by using the proposed model and FEAP finite beam, with the same mesh density with 14 beam elements.

The obtained responses are compared with the analytical solution (Fig. 7(a)), showing good matching between the results computed by the proposed beam model against the analytical solution. In order to present the performance of the proposed beam model, we have computed the same shallow beam with assumed constitutive parameters related to plasticity (Fig. 6). The assumed constitutive parameters trigger plasticity only in axial response. The comparison of elasto-plastic vs. elastic response (Fig. 4(b)) shows a significant difference between the two responses.

Constitutive parameters:
$E = 19971.4; A = 0.4083$
$I = 0.0133$
Assumed:
$N_y = 0.9799; \quad M_y = 1.0435$
$K_h = 0.1E$
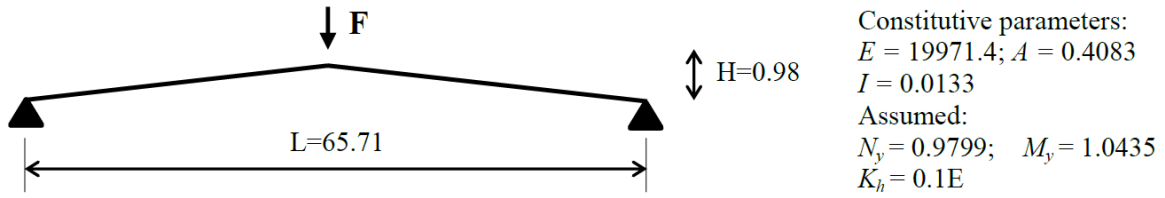
Fig. 6 Geometry of Williams toggle frame
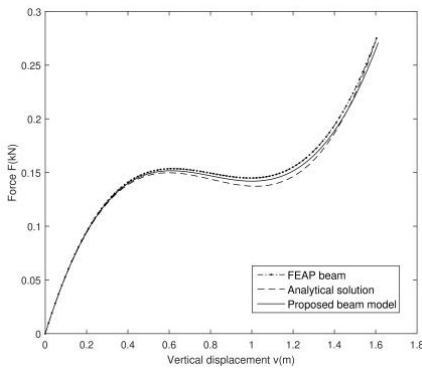
(a) FEAP beam vs. analytical solution vs. proposed model
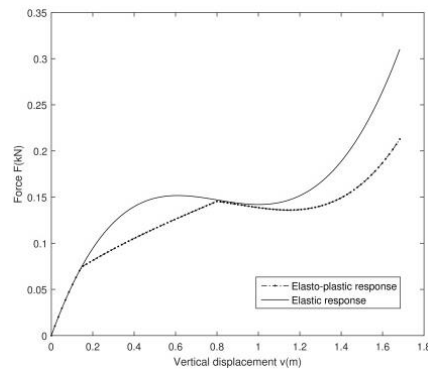
(b) Elastic vs. elasto-plastic response

Fig. 7 Responses comparison
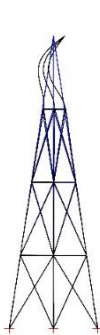
(a) First buckling mode (Linear buckling analysis)
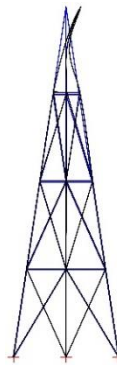
(b) Deformed shape in time when instability occurs (Finite strain analysis)
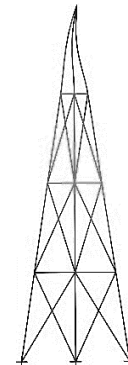
(c) Deformed shape in time when instability occurs (our model)

Fig. 8 Stability analysis of the tower

Table 2 Comparison of the critical force and vertical displacement values

	Analysis type	Linear buckling	Finite strain	Our model
$A = 0.00538 \ m^2$ $I = 6.04\text{E-}06 \ m^4$	$F_{cr} \ [kN]$	16439.0	16175.0	16360.0
	$v_{cr} \ [m]$	-2.517E-02	-2.558E-02	-2.577E-02
$A = 11.75\text{E-}04 \ m^2$ $I = 107.22\text{E-}08 \ m^4$	$F_{cr} \ [kN]$	2989.60	2923.80	2959.40
	$v_{cr} \ [m]$	-2.097E-02	-2.116E-02	-2.134E-02
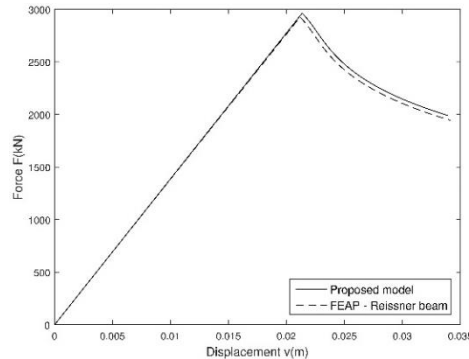
Fig. 9 Response of the tower

4.3 Tower analysis

In order to validate our model in the computation of more complex structures, we will perform a stability analysis of a tower, which was analyzed in Ibrahimbegovic *et al.* (2013) using linear buckling and finite strain model, and also in Ngo *et al.* (2014). The vertical force is applied at top of the tower, as well as small horizontal perturbation force. The comparison of the deformed shape in time when instability occurs, using finite elements described here, to the buckling mode and to the deformed shape of the tower from Ibrahimbegovic *et al.* (2013), is given in Fig. 8.

Obtained values of the critical force values and corresponding vertical displacement of the node at the top of the tower are summarized in Table 2. Our model gives the critical force value between values computed using linear buckling and finite strain model. Displacement values are almost the same in all three analyses. We can conclude that the proposed model can be used in the stability analysis of the different types of structures.

Next, we make the tower more flexible by using reduced values of the cross-sectional properties, while keeping the height and the span of the tower the same. The obtained results of the critical force and corresponding displacement are shown in Table 2.

In Fig. 9, we give the response of the tower for two analyses, where F is vertical force applied at the node at top of the tower, and v is the vertical displacement of the same node. We can see a very good match between these two results.

Furthermore, we want to test the behavior of the tower in the elasto-plastic regime. The constant vertical force is applied at the top of the tower while increasing horizontal force is acting at the same point (Fig. 10(a)). In Fig. 10(b) we give the comparison between the tower response in elasticity and in elastoplasticity. The force in Fig. 10(b) denotes the horizontal force at the node at top of the tower, and the displacement is the horizontal displacement of the same node.

4.4 Cable structure under dead load

This example is adopted from the reference work Ibrahimbegovic (1992) in order to test the accuracy of our formulation for static analysis of a cable structure. We observe a straight cable structure in the reference configuration with pretensioned force $P=20000$, which is applied imposing displacement of support $\Delta u=51$. The span of the cable structure is $L=20000$ and Young's modulus is $E=2 \cdot 10^8$. The round cross-section is assumed, while the radius $R=0.288$ is calculated from the cross-section area $A=0.065$.

(a) Geometry and the constitutive parameters

Constitutive parameters:
$EA = 2.2E+07$;
$EI = 388.0$;
$N_y = 240.0$;
$M_y = 15.2$;
$K_h = 0.1E$

(b) Elastic vs. elasto-plastic response of the tower
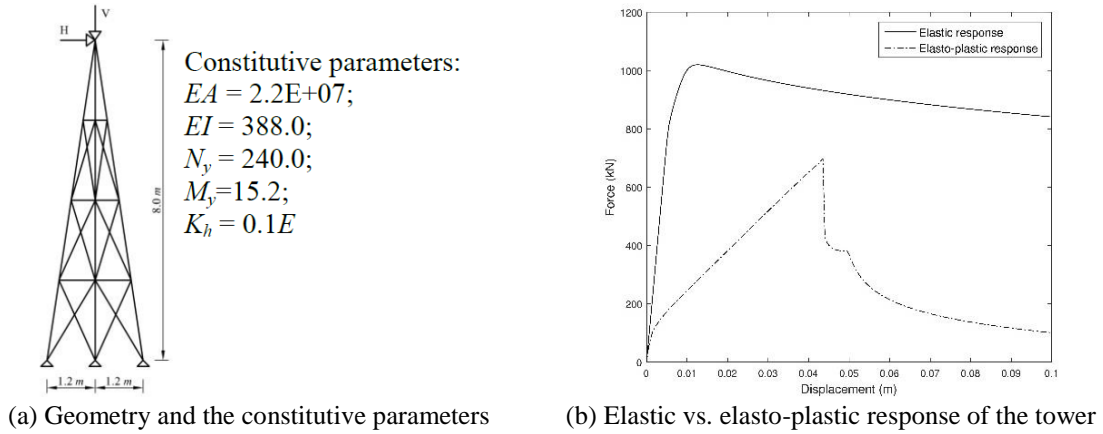
Fig. 10 Pushover analysis of the tower

Material and geometric charact.:
$L = 100\ m$
$A = 2.88E\text{-}04\ m^2$
$E = 7.75E+07\ kN/m^2$
Utimate stress and stress resultant:
$\sigma_{u,t} = 3.96E+06\ kN/m^2$
$N_{u,t} = 114\ kN$
Vertical load – force:
$P = 22\ kN$
Pretension force:
$N_{p,t} = 0.7N_{u,t} = 79.8\ kN$
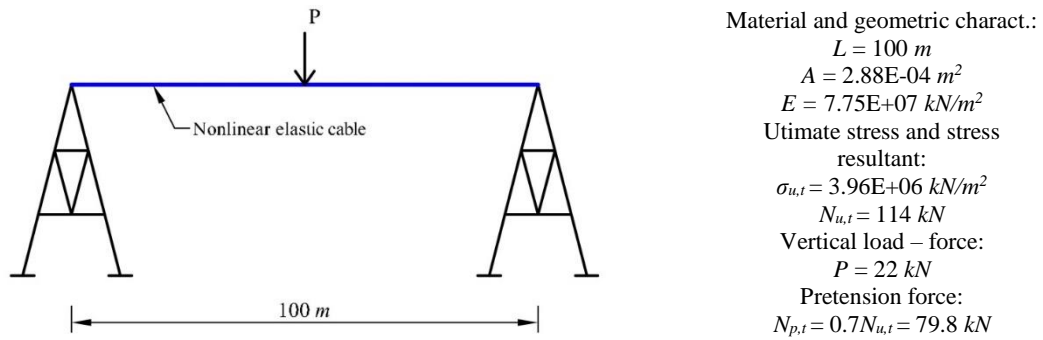
Fig. 11 Material and geometric characteristics of the power line

(a) Two tension towers

(b) Tension and transition tower
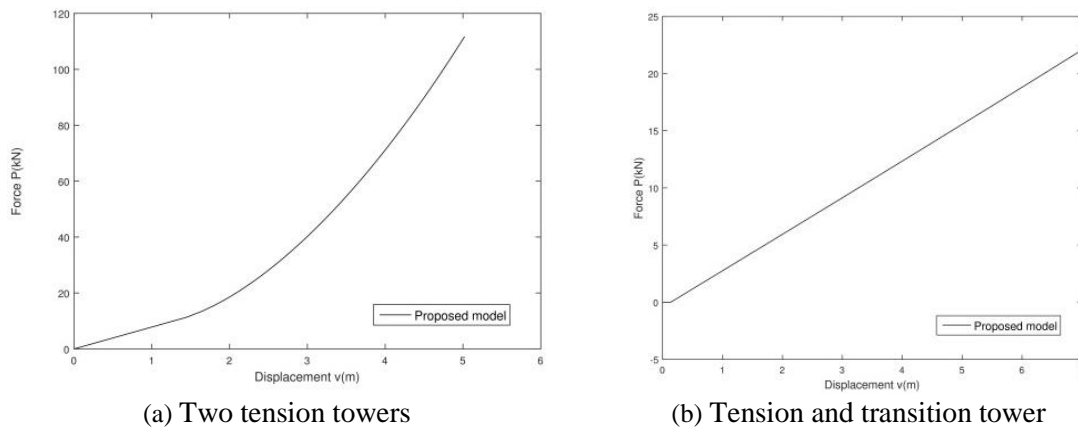
Fig. 12 Response of power line–cable response

The reference solution of the vertical displacement in the middle of span is $v=292.6863$, while the proposed formulation of Kirchhoff beam results with $v=293.23$, which demonstrates an excellent performance for analysis of a cable structure.

4.5 Cable structure – Power line between two transmission tower

In this example, we present an application of the proposed beam model to the cable structure, such as a power line between two transmission towers. Namely, it is known, a few transmission tower types exist, such as the tension tower and the transition tower. In power line (cable) analysis, the first type can be model with fixed support, and the second with sliding support.

Our model can be used in the cable computation when both ends are fixed, or when one end is fixed and the other one is sliding support. The first case can be interesting in the design of a cable section. The second is useful in computing deflection of the cable (power line), and it depends on prestress force acting at the sliding end of the cable. The results of the computations are shown in Fig. 12.

5. Conclusions

In this paper, we have presented theoretical formulation and numerical implementation of geometrically exact initially curved beam model including Kirchhoff's kinematics constraint of vanishing shear deformation. The formulation has been derived from Reissner's beam model theory imposing Kirchhoff's constraint on a particular choice of shear deformation measure in terms of rotated strain. The same choice of strain measure allows us to develop the constitutive law of plasticity with linear hardening, with the corresponding yield criterion applied separately for axial force and bending moment.

The finite element approximation is constructed by using Hermite's polynomials for both position vector and displacement components, providing smoothness between two elements. Through several numerical simulations, we have demonstrated an excellent performance of the proposed beam model. The model is able to deal with buckling and post-buckling analysis of thin beam structure and cable structure, also accounting for nonlinear material behavior.

Acknowledgments

References

Armero, F. and Valverde, J. (2012), "Invariant Hermitian finite elements for thin Kirchhoff rods. II: The linear three-dimensional case", *Comput. Meth. Appl. Mech. Eng.*, **213-216**, 458-85. https://doi.org/10.1016/j.cma.2011.05.014.

Boyer, F. and Primault, D. (2004), "Finite element of slender beams in finite transformations: A geometrically exact approach", *Int. J. Numer. Meth. Eng.*, **59**, 669-702. https://doi.org/10.1002/nme.879.

DaDeppo, D.A. and Schmidt, R. (1975), "Instability of clamped-hinged circular arches subjected to a point load", *J. Appl. Mech.*, **42**(4), 894-96. https://doi.org/10.1115/1.3423734.

Hadzalic, E., Ibrahimbegovic, A. and Dolarevic, S. (2018), "Failure mechanisms in coupled soil-foundation systems", *Coupled Syst. Mech.*, **7**(1), 27-42. https://doi.org/10.12989/csm.2018.7.1.027.

Hadzalic, E., Ibrahimbegovic, A. and Nikolic, M. (2018), "Failure mechanisms in coupled poro-plastic

medium", *Coupled Syst. Mech.*, **7**(1), 43-59. https://doi.org/10.12989/csm.2018.7.1.043.

Hill, R. (1950), *The Mathematical Theory of Plasticity*, Clarendon Press, Oxford, U.K.

Ibrahimbegovic, A. (1992), "A consistent finite-element formulation of non-linear elastic cables", *Commun. Appl. Numer. Meth.*, **8**(8), 547-556. https://doi.org/10.1002/cnm.1630080809.

Ibrahimbegovic, A. (1995), "On finite element implementation of geometrically nonlinear Reissner's beam theory: Three-dimensional curved beam elements", *Comput. Meth. Appl. Mech. Eng.*, **122**(1-2), 11-26. https://doi.org/10.1016/0045-7825(95)00724-F.

Ibrahimbegovic, A. (2009), *Nonlinear Solid Mechanics*, Springer, Dordrecht, Germany.

Ibrahimbegovic, A. and Frey, F. (1993a), "Finite element analysis of linear and non-linear planar deformations of elastic initially curved beam", *Int. J. Numer. Meth. Eng.*, **36**, 3239-3258. https://doi.org/10.1002/nme.1620361903.

Ibrahimbegovic, A., Hajdo, E. and Dolarevic, S. (2013), "Linear instability or buckling problems for mechanical and coupled thermomechanical extreme conditions", *Coupled Syst. Mech.*, **2**(4), 349-374. https://doi.org/10.12989/csm.2013.2.4.349.

Imamovic, I., Ibrahimbegovic, A. and Mesic, E. (2017), "Nonlinear kinematics Reissner's beam with combined hardening/softening elastoplasticity", *Comput. Struct.*, **189**, 17-20. https://doi.org/10.1016/j.compstruc.2017.04.011.

Imamovic, I., Ibrahimbegovic, A. and Mesic, E. (2018), "Coupled testing-modeling approach to ultimate state computation of steel structure with connections for statics and dynamics", *Coupled Syst. Mech.*, **7**(5), 555-581. https://doi.org/10.12989/csm.2018.7.5.555

Imamovic, I., Ibrahimbegovic, A., Knopf-Lenoir, C. and Mesic, E. (2015), "Plasticity-damage model parameters identification for structural connections", *Coupled Syst. Mech.*, **4**(4), 337-364. https://doi.org/10.12989/csm.2015.4.4.337.

Kitarovic, S. (2014) "Nonlinear Euler–Bernoulli beam kinematics in progressive collapse analysis based on the Smith's approach", *Mar. Struct.*, **39**, 118-130. https://doi.org/10.1016/j.marstruc.2014.07.001.

Maassen, S., Pimenta, P. and Schröeder, J. (2018), "A geometrically exact euler-bernoulli beam formulation for nonlinear 3d material laws", *Proceedings of the 39th Ibero-Latin American Congress on Computational Methods in Engineering*, Paris/Compiègne, France, November.

Maurin, F., Greco, F., Dedoncker, S. and Desmet, W. (2018), "Isogeometric analysis for nonlinear planar Kirchhoff rods: Weighted residual formulation and collocation of the strong form", *Comput. Meth. Appl. Mech. Eng.*, **340**, 1023-1043. https://doi.org/10.1016/j.cma.2018.05.025.

Meier, C., Grill, M.J., Wall, W. and Popp, A. (2018), "Geometrically exact beam elements and smooth contact schemes for the modeling of fiber-based materials and structures", *Int. J. Solids Struct.*, **154**, 124-46. https://doi.org/10.1016/j.ijsolstr.2017.07.020.

Meier, C., Popp, A. and Wall, W. (2019), "Geometrically exact finite element formulations for slender beams: Kirchhoff-love theory versus Simo-Reissner theory", *Arch. Comput. Meth. Eng.*, **26**(1), 163-243. https://doi.org/10.1007/s11831-017-9232-5.

Ngo, V.M., Ibrahimbegovic, A. and Hajdo, E. (2014), "Nonlinear instability problems including localized plastic failure and large deformations for extreme thermo-mechanical conditions", *Coupled Syst. Mech.*, **3**(1) ,89-110. https://doi.org/10.12989/csm.2014.3.1.089.

Pirmanšek, K., Češarek, P., Zupan, D. and Saje, M. (2017), "Material softening and strain localization in spatial geometrically exact beam finite element method with embedded discontinuity", *Comput. Struct.*, **182**, 267-283. https://doi.org/10.1016/j.compstruc.2016.12.009.

Reissner, E. (1972), "On one-dimensional finite-strain beam theory: The plane problem", *Zeitschrift für angewandte Mathematik und Physik ZAMP*, **23**(5), 795-804. https://doi.org/10.1007/BF01602645.

Reissner, E. (1981), "On finite deformations of space-curved beams", *Zeitschrift für angewandte Mathematik und Physik ZAMP*, **32**(6), 734-44. https://doi.org/10.1007/BF00946983.

Simo, J.C. (1985), "A finite strain beam formulation. The three-dimensional dynamic problem. Part I. Computer", *Meth. Appl. Mech. Eng.*, **49**(1), 55-70. https://doi.org/10.1016/0045-7825(85)90050-7.

Simo, J.C., Hjelmstad, K.D. and Taylor, R.L. (1984), "Numerical formulations of elasto-viscoplastic response of beams accounting for the effect of shear", *Comput. Meth. Appl. Mech. Eng.*, **42**(3), 301-330.

https://doi.org/10.1016/0045-7825(84)90011-2.

Sonneville, V., Brüls, O. and Bauchau, O. (2017), "Interpolation schemes for geometrically exact beams: A motion approach", *Int. J. Numer. Meth. Eng.*, **112**(9), 1129-53. https://doi.org/10.1002/nme.5548.

Taylor, R.L. (2008), *FEAP - A Finite Element Analysis Program*, Berkeley, California, U.S.A.

Williams, F.W. (1964), "An approach to the non-linear beahviour of the members of a rigid jointed plane framework with finite deflection", *Quart. J. Mech. Appl. Math.*, **17**(4), 451-469. https://doi.org/10.1093/qjmam/17.4.451.

AI